Search for shape-isomers in the Pt-Hg-Pb region

J. Bartel,[1,*] H. Molique,[1] B. Nerlo-Pomorska,[2] M. Warda,[2] and K. Pomorski[3]

[1] *D.R.S. Institut Pluridisciplinaire Hubert Curien, CNRS-IN2P3, Université de Strasbourg, Strasbourg, France*
[2] *Department of Theoretical Physics, Maria Curie-Skłodowska University, Lublin, Poland*
[3] *National Centre for Nuclear Research, Warsaw, Poland*

(Dated: February 10, 2025)

Potential energy surfaces of nine even-even isotopes of Pt, Hg, and Pb around ^{186}Pt are evaluated within a macroscopic-microscopic model based on the Lublin-Strasbourg-Drop macroscopic energy and the microscopic energy obtained using the Yukawa-folded mean-field potential to establish the Strutinski shell corrections and the pairing correlation energy through the BCS approach with a monopole pairing force. The rapidly converging Fourier-over-Spheroid shape parametrization is used to describe nuclear deformations. The stability of the shape isomeric states and the possibility of a shape coexistence with respect to non-axial and higher-order deformations is investigated.

KEYWORDS: macro-micro model, shape coexistence, shape isomers.

PACS numbers: 21.10.Dr, 21.10.Ma, 21.60.Cs, 21.60.Jz, 25.85.Ca

I. INTRODUCTION

Our understanding of shape isomerism and shape coexistence in nuclei has substantially changed over the last decades. Even though shape isomers were discovered in the 1960s in connection with investigations of fissioning systems [1], their existence was long understood as an exotic phenomenon limited to different islands in the nuclear chart. The present understanding, however, is the one of the occurrence of such states in nuclei all along the nuclear chart, with the only exception of very light nuclei [2–7]. The existence in ^{66}Ni, to give just one prominent example, of (prolate as well as oblate) isomeric states has been identified both through the experiment (see, e.g., Ref. [8, 9] and references therein) and a large variety of very different theoretical models [10, 11] ranging from mean-field calculations of the Hartree-Fock + BCS or Hartree-Fock-Bogoliubov type to macroscopic-microscopic approaches [12, 13], to Monte-Carlo Shell-Model calculations of the Takaharu Otsuka group [14] or Shell Model calculations with LNPS interaction of the Madrid-Strasbourg group [15].

The region just below the $Z = 82$ shell closure (Platinum, Mercury, and Lead) has already been identified some time ago in different studies [16–21] as one of the most favorable for the occurrence of shape coexistence. This discovery has strongly motivated theoretical studies to explore this region of nuclei in more detail. Important advances in the study of neutron-deficient nuclei around $Z \approx 82$ have been realized using shape isomers and β-decays of nuclei populated by relativistic energy-fragmentation experiments [22] performed at GSI within the RISING campaign or through tagging techniques at the Accelerator Laboratory of the University of Jyväskylä (Finland) [23], and through Coulomb-excitation experiments undertaken at the REX-ISOLDE facility in CERN [24].

Interesting theoretical studies on this subject, based either on a self-consistent approach (see, e.g., Refs. [19, 25–27]) or on macroscopic-microscopic (e.g., [12, 13, 28]) models, have been published in the past.

The aim of the current paper is to study the influence on the potential energy surfaces (PES) of even-even Pt, Hg, and Pb isotopes around ^{186}Hg of higher-order deformations that go beyond a simple quadrupole shape using our recently developed and very efficient Fourier-over-Spheroid (FoS) shape parametrization [29, 30], together with the macroscopic-microscopic (mac-mic) approach with the Lublin-Strasbourg Drop (LSD) [31], able to reproduce accurately both nuclear masses and fission barriers, and a Yukawa-folded single-particle potential [32, 33] to account for shell and pairing-energy corrections. The results will be compared with outcome of the self-consistent calculations performed in the Hatree-Fock-Bogoliubov (HFB) theory with Gogny D1S force [44] .

Although the investigations of the nuclear potential-energy surfaces presented in a previous study [28] had been carried out for a broader range of nuclei in a similar approach, some new effects are included in the present work through the new *Fourier over spheroid* shape parametrization which enables us, in particular, to project the evaluated PES onto the traditional (β, γ) plane. In addition, higher-order deformation parameters are taken into account here, still keeping the 60° symmetry of the original (β, γ) parametrization.

II. SHAPES BREAKING AXIAL SYMMETRY

A search of possible shape isomers is carried out in the Pt, Hg, Pb (Z=78, 80, 82) region by studying the

*Electronic address: Johann.Bartel@iphc.cnrs.fr

landscapes in the deformation-energy space of different even-even isotopes of each of these nuclei. The calculation of the nuclear energy as a function of the chosen deformation parameters is performed in the framework of the macroscopic-microscopic approach with the LSD model [31] for the macroscopic term and the shell and pairing energy corrections evaluated using the Yukawa-folded mean-field potential [32] for the microscopic part. To be able to have at our disposal a most flexible description of the nuclear deformation, we use the Fourier shape parametrization [34] in the form of what we call the "Fourier over Spheroid" definition [29, 30] with a deformation space spanned by four parameters $\{c, \eta, a_3, a_4\}$ which stand respectively for elongation, non-axiality, left-right asymmetry, and neck (hexadecapole) degree of freedom.

Our aim is to show that this deformation space is in a way equivalent to the widely known and used Bohr $\{\beta, \gamma\}$ shape parametrization [35], though allowing for substantially more general deformations. An ellipsoid can, indeed, be generally described in cartesian coordinates by three half-axis $\mathcal{A}_i$, $\mathcal{A}_j$ and $\mathcal{A}_k$ through the equation

$$\frac{x^2}{\mathcal{A}_1^2} + \frac{y^2}{\mathcal{A}_2^2} + \frac{z^2}{\mathcal{A}_3^2} = 1 \ . \tag{1}$$

If all the half-axis are different, one speaks about a Jacobi spheroid (symmetry group D_{2h}). If two of the half-axis are the same, like $\mathcal{A}_1 = \mathcal{A}_2$, the spheroid has a symmetry axis. One then speaks about a spheroid of revolution, which can be prolate or oblate (Maclaurin spheroid). Instead of the half-axis $\mathcal{A}_\nu$, one then introduces deformation parameters β and γ through

$$\mathcal{A}_\nu = R(\beta,\gamma)\left[1 + k\,\cos(\gamma - \frac{2\pi}{3}\nu)\right] \ , \quad \nu = 1,2,3 \tag{2}$$

where $k = \sqrt{\frac{5}{4\pi}}\beta$ and where

$$R(\beta,\gamma) = R_0\left[1 - \frac{3}{4}k^2 + \frac{k^3}{4}\cos(3\gamma)\right]^{-1/3} \tag{3}$$

with R_0 being the radius of the spherical shape and where volume conservation requires that $\frac{4\pi}{3}\mathcal{A}_1\mathcal{A}_2\mathcal{A}_3 = \frac{4\pi}{3}R_0^3$.

The Bohr parametrization allows to describe non-axial spheroidal shapes with two deformation parameters, β for its elongation and γ, an angle that takes care of the orientation of the spheroid, as illustrated in Fig. 1. The above equations show that $\beta = 0$ corresponds to the spherical shape. Along the abscissa ($\gamma{=}0°$), one has a prolate deformation with z (or 3) as the symmetry axis, while for $\gamma = 60°$ the shape is oblate with y (or 2) as the symmetry axis. The $\{\beta, \gamma\}$ plane is then symmetric in $\gamma = 60°$ portions so that the shape with $\gamma = 120°$ is identical to the one with $\gamma = 0°$ except that the profile is now symmetric through rotations about the x (or 1) axis which is the symmetry axis. An identical nuclear deformation appears 3 times, each time at an interval of 120 degrees

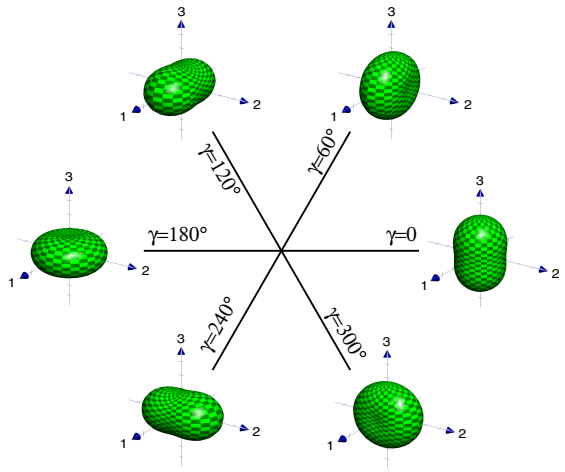

FIG. 1: Illustration of the symmetry of Bohr's $\{\beta, \gamma\}$ shape parametrization.

with a symmetry axis, which is respectively the 1, 2 or 3-axis.

If higher order, such as hexadecapole deformations, need to be included, this 60° symmetry is broken, and a given $\{\beta, \gamma\}$ deformation is no longer the same (not even with a different orientation) as the corresponding $\{\beta, \gamma{+}120°\}$, or $\{\beta, \gamma{+}240°\}$ deformation. This is, however, the difficulty that one encounters when trying to represent a nuclear shape obtained in the Fourier shape parametrization [29, 34] in the framework of the Bohr $\{\beta, \gamma\}$ deformation space and, also in the Rayleigh type expansions of nuclear surface (confer, e.g., Ref. [36]).

Instead of limiting oneself to the $0 \leq \gamma \leq 60°$ sector and exploring, for a given deformation point, higher-order deformations, one performs calculations of the potential-energy surface (PES) in all three sectors $0 < \gamma < 60°$, $60° < \gamma < 120°$, $120° < \gamma < 180°$, which basically means that one starts from a particular nuclear shape, but oriented differently in space, and investigates which is the orientation where the addition of higher order deformations leads to the minimal energy. In this way, one restores the initial symmetry of the three sectors, allowing us to obtain what we can call the "*symmetrized potential energy surface*" (SPES), which we will discuss in the present study.

In order to illustrate the method, we show in Fig. 2 the direct (upper part) and the symmetrized potential energy (lower part) surfaces obtained for the ^{186}Hg isotope, when restricting the study to left-right symmetric shapes (with deformation parameter $a_3 = 0$) and minimized with respect to the hexadecapole parameter a_4 [34]. Energy labels on these and subsequent figures always indicate the total nuclear energy relative to the spherical macroscopic energy. One notices in particular in the lower part of the figure the symmetry of the three

sectors delimited by the lines $\gamma = 60°$ and $\gamma = 120°$ two of which then obviously become redundant.

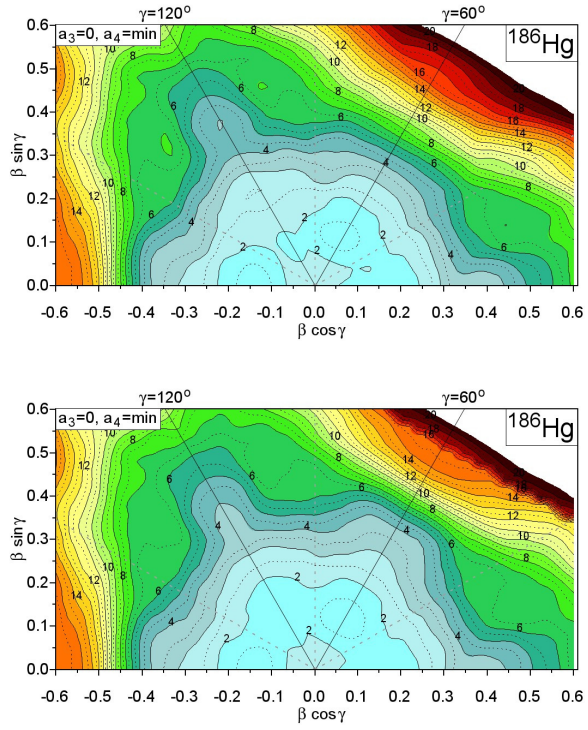

FIG. 2: Potential energy surface (PES) obtained in the tree (β, γ) sectors (upper map) and symmetrized potential-energy surface (SPES) (lower map) for the ^{186}Hg nucleus obtained by the symmetrization procedure as explained in the text.

A. Macroscopic-microscopic model

In the mac-mic method, proposed first by Myers and Świątecki [37], the total energy of the deformed nucleus is equal to the sum of a macroscopic (liquid-drop type) energy and the quantum energy correction for protons and neutrons generated by shell and pairing effects

$$E_{\rm tot} = E_{\rm LSD} + {\rm E}_{\rm shell} + {\rm E}_{\rm pair} \ . \tag{4}$$

The LSD model [31], which reproduces well all experimental masses and fission barrier heights, is used in this study to evaluate the macroscopic part of the energy. The shell corrections are obtained by subtracting the average energy $\widetilde{E}$ from the sum of the single-particle (s.p.) energies of occupied orbitals

$${\rm E}_{\rm shell} = \sum_k e_k - \widetilde{E} \ . \tag{5}$$

As the s.p. energies e_k, we have taken the eigenvalues of a mean-field Hamiltonian with the Yukawa-folded s.p. potential [32]. The average energy $\widetilde{E}$ is evaluated using the Strutinsky prescription [38, 39] with a $6^{\rm th}$ order correction polynomial. The pairing energy correction is determined as the difference between the BCS energy [40] and the s.p. energy sum from which the average pairing energy [39] is subtracted

$$E_{\rm pair} = E_{\rm BCS} - \sum_k e_k - \widetilde{E}_{\rm pair} \ . \tag{6}$$

In the BCS approximation, the ground-state energy of a system with an even number of particles is given by

$$E_{\rm BCS} = \sum_{k>0} 2e_k v_k^2 - G(\sum_{k>0} u_k v_k)^2 - G\sum_{k>0} v_k^4 - \mathcal{E}_0^{\varphi} \ , \tag{7}$$

where the sums run over the pairs of s.p. levels belonging to the pairing window defined below. The coefficients v_k and $u_k = \sqrt{1 - v_k^2}$ are the BCS occupation amplitudes, and $\mathcal{E}_0^{\varphi}$ is the energy correction due to the particle number projection done in the GCM+GOA approximation [41]

$$\mathcal{E}_0^{\varphi} = \frac{\sum\limits_{k>0} [(e_k - \lambda)(u_k^2 - v_k^2) + 2\Delta u_k v_k + G v_k^4]/E_k^2}{\sum\limits_{k>0} E_k^{-2}} \ . \tag{8}$$

Here $E_k = \sqrt{(e_k - \lambda)^2 + \Delta^2}$ are the quasi-particle energies with Δ and λ the pairing gap and the Fermi energy, respectively. The average projected pairing energy, for a pairing window of width 2Ω, symmetric in energy with respect to the Fermi level, is equal to

$$\begin{aligned} \widetilde{E}_{\rm pair} = & -\frac{\tilde{g}}{2}\,\tilde{\Delta}^2 + \frac{\tilde{g}}{2}\,G\tilde{\Delta}\arctan\left(\frac{\Omega}{\tilde{\Delta}}\right) - \log\left(\frac{\Omega}{\tilde{\Delta}}\right)\tilde{\Delta} \\ & + \frac{3}{4}G\frac{\Omega/\tilde{\Delta}}{1 + (\Omega/\tilde{\Delta})^2}/\arctan\left(\frac{\Omega}{\tilde{\Delta}}\right) - \frac{1}{4}G \ , \end{aligned} \tag{9}$$

where $\tilde{g}$ is the average single-particle level density and $\tilde{\Delta}$ the average pairing gap corresponding to a pairing strength G

$$\tilde{\Delta} = 2\Omega \exp\left(-\frac{1}{G\tilde{g}}\right) \ . \tag{10}$$

The pairing window for protons or neutrons contains $2\sqrt{15\mathcal{N}}$ ($\mathcal{N}$ = N or Z) s.p. levels closest to the Fermi energy states. For such a window, the paring strength approximated in Ref. [42] is given by the following expression:

$$G = \frac{g_0}{\mathcal{N}^{2/3}\,A^{1/3}} \ . \tag{11}$$

The same value $g_0 = g_0^p = g_0^n = 0.28\hbar\omega_0$ is taken for protons and neutrons, where $\hbar\omega_0 = 41\,{\rm MeV}/A^{1/3}$ is the nuclear harmonic oscillator constant.

In our calculation, the single-particle spectra are obtained by diagonalization of the s.p. Hamiltonian with the Yukawa-folded potential [32, 33] with the same parameters as used in Ref. [43].

III. SPES'S OF SELECTED PT, HG, AND PB ISOTOPES

We show in Figs. 3, 4 and 5 the symmetrized potential energy surfaces for the Pt, Hg, and Pb isotopes, obtained in the full 3-dimensional deformation space, but then minimized with respect to the neck a_4 parameter and projected on the traditional [35] $(\beta\cos\gamma, \beta\sin\gamma)$ plane. We have indeed found that the influence of the left-right asymmetry parameter a_3 for the SPESs of the considered nuclei is negligible at small deformations $\beta < 0.6$. All maps, except when considering very elongated shapes towards the end of our study (section 4), are therefore shown for $a_3 = 0$.

For the platinum isotopes ^{182}Pt up to ^{186}Pt, a broad ground-state (g.s.) minimum is clearly visible at $\beta \approx 0.15$ and $\gamma = 0$, and an oblate isomeric state ($\gamma = 60°$) at slightly larger β value. A barrier of approximately 0.5 MeV separates both minima. Please note that, for practical reasons, we represent in all the figures the full range $\gamma = 0 - 90°$, where the symmetry of these figures with respect to the $\gamma = 60°$-line should be noticed. When comparing the SPES of the three platinum isotopes shown here, one observes the emergence of some "*valley*" that extends between $\beta \approx 0.4$ and 0.5 along the prolate axis. Such a valley will also be observed, even more pronounced, in the mercury and lead isotopes discussed below. In ^{186}Pt, some bump emerges at $\{\beta \approx 0.43, \gamma \approx 20°\}$ the appearance of which could already be expected when looking at the SPES of the ^{184}Pt nucleus.

For the mercury isotope ^{184}Hg, the picture is again about the same as for the platinum nuclei with a broad minimum clearly visible at $\beta \approx 0.15$, with the difference, however, that the ground state now evolves, with increasing mass number, to an oblate deformation ($\gamma = 60°$). The prolate minima at $\beta \approx 0.2$ are visible in ^{184}Hg and ^{186}Hg isotopes. A very small barrier separates both prolate and oblate minima, which disappears in ^{188}Hg. In ^{184}Hg, a shallow shape isomer appears; in addition, at $\{\beta \approx 0.46, \gamma \approx 27°\}$ around 6 MeV above the g.s. Similar non-axial isomeric states are also found in the two other mercury isotopes. In ^{188}Hg an additional shape isomer appears at $\{\beta \approx 0.52, \gamma \approx 20°\}$. Some broad prolate valley develops around 4 MeV above the g.s. in all three Hg isotopes at $\beta \approx 0.35$, as already observed in the Pt nuclei, valley which stretches to larger β values as the neutron number increases.

The broad minimum along $\beta \approx 0.15$ observed for the platinum and mercury isotopes disappears in the lead nuclei from ^{186}Pb up to ^{190}Pb, in which the ground-state minimum appears at the spherical shape ($\beta = 0$) and which becomes gradually deeper as the mass number increases and one approaches the doubly magic ^{208}Pb. Please notice that there is a small oblate ($\gamma = 60°$) depression that appears in ^{186}Pb at $\beta \approx 0.38$. The valley along the prolate axis that has already been observed at an elongation between $\beta = 0.4$ and $\beta = 0.5$ now leads in ^{188}Pb and ^{190}Pb nuclei to a clearly defined shape isomeric state at about 3 MeV above the ground state. In addition, an oblate local minimum is found in the ^{190}Pb isotope at $\beta = 0.18$ and an energy of about 1.5 MeV.

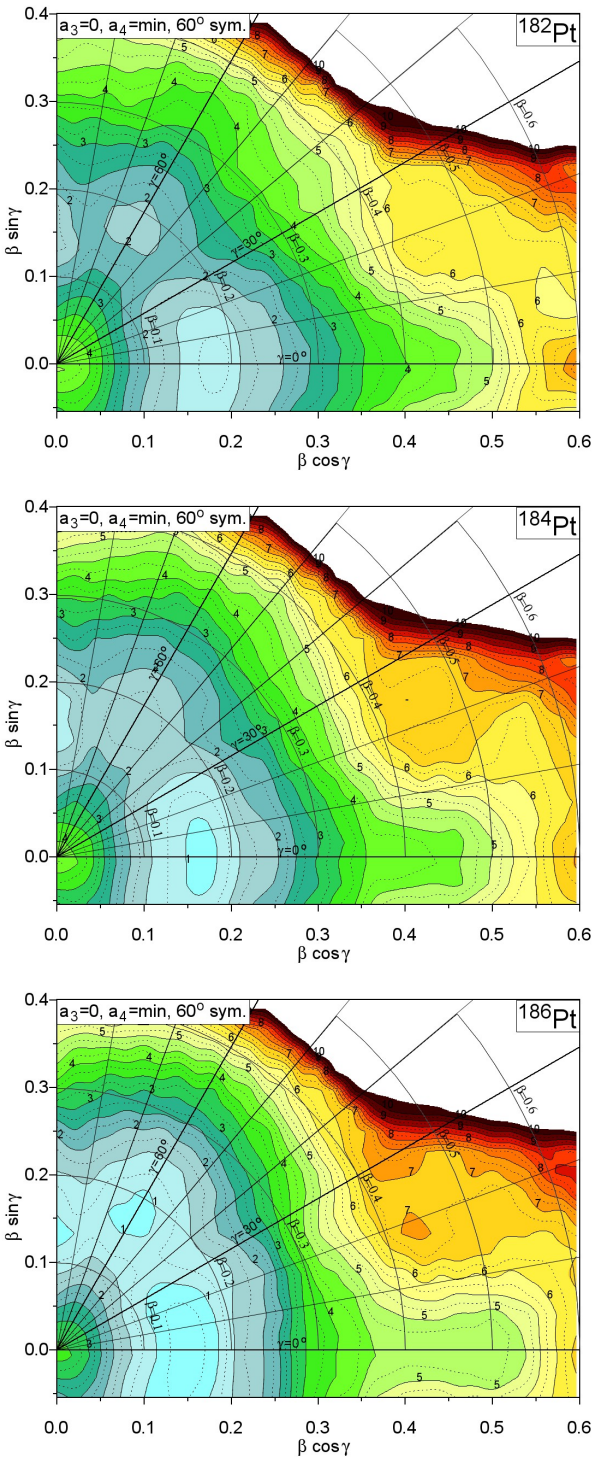

FIG. 3: Symmetrized potential energy surfaces for Pt isotopes.

The question now arises as to how reliable our estimates really are. Trying to give an answer, we have

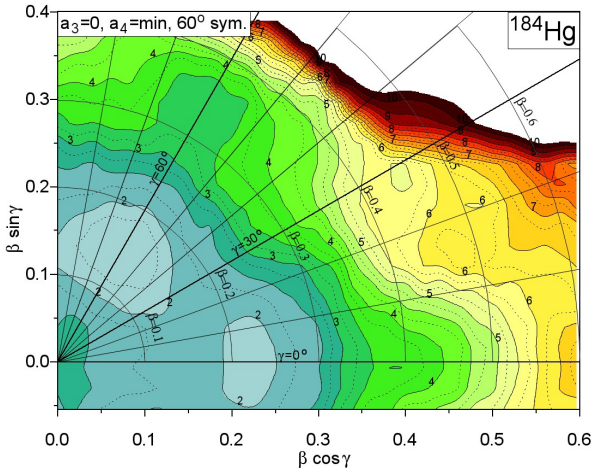

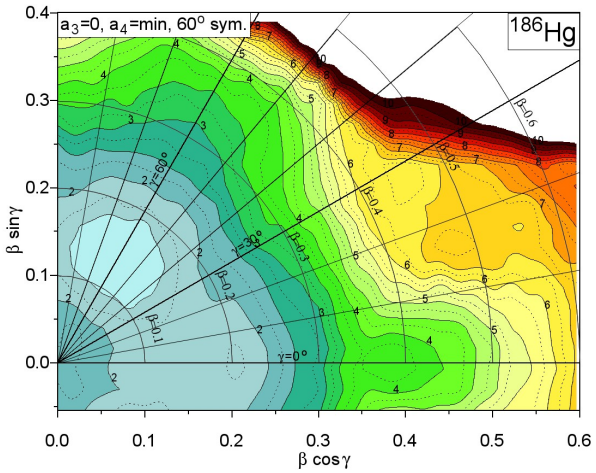

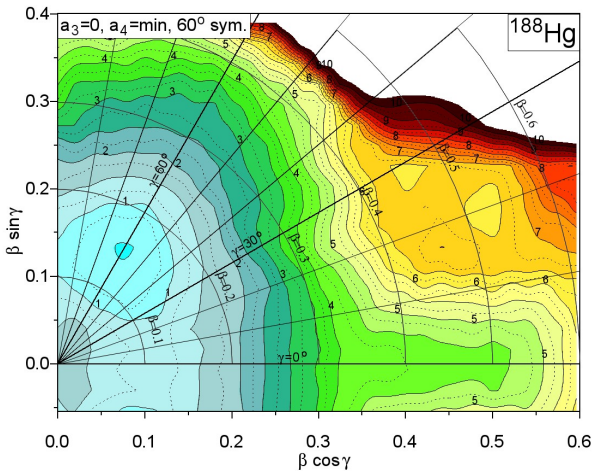

FIG. 4: Symmetrized potential energy surfaces for Hg isotopes.

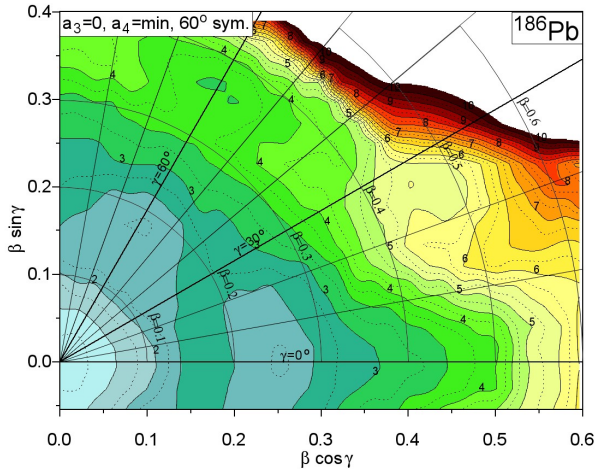

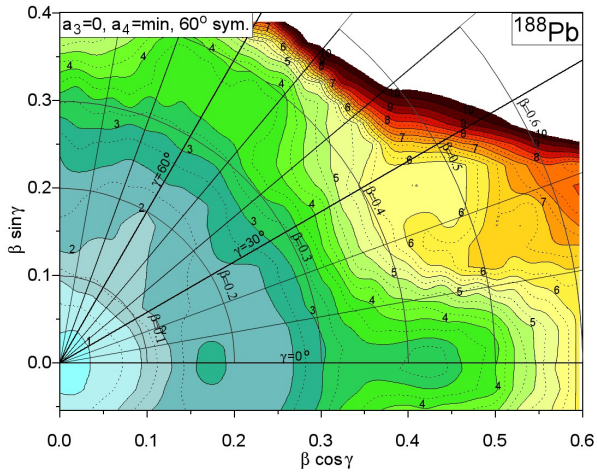

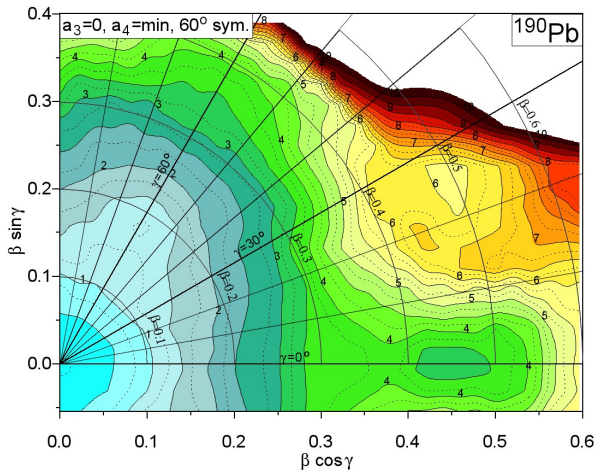

FIG. 5: Symmetrized potential energy surfaces for Pb isotopes.

performed for the isotope ^{186}Hg a self-consistent constrained HFB calculation with the Gogny D1S force [44] using as a constraint the axial Q_{20} and non-axial Q_{22} mass quadrupole moments. This method allowed to show the important role of triaxial deformation in the ground state shape of nuclei from the Pt region [46, 47]. The corresponding PES is shown in the lower part of Fig. 6. In the HFB calculation, the ground state is found for an essentially prolate shape with a slight triaxiality of about $\gamma = 12°$, about 200 keV lower than the oblate

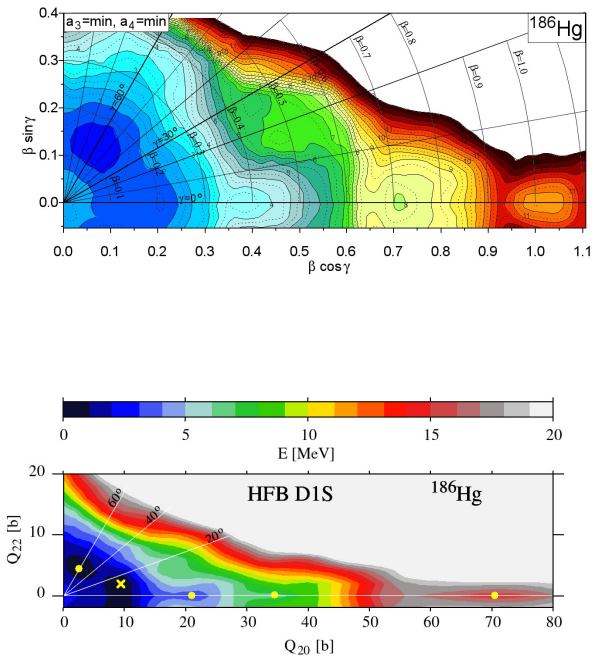

FIG. 6: Potential energy surface of ^{186}Hg evaluated within the macroscopic-microscopic approach (upper part) and, for comparison, in the HFB approach with the Gogny D1S force [44] (lower part), using constraints on the axial Q_{20} and non-axial Q_{22} mass quadrupole moments. Yellow dots mark local minima and the ground state is indicated by a cross.

minimum. In the macroscopic-microscopic approach, the ground state is found, on the contrary, to be oblate deformed, about 300 keV lower than the prolate minimum (upper part of Fig. 6). In both calculations, several prolate local minima are found. HFB calculations show these at $Q_{20} \approx 21.0$, 34.4 and 70.5b, corresponding respectively to a value of $\beta = 0.56$, 0,79 and 1,13 in the macroscopic-microscopic calculation, obtained from a rough estimate

$$\beta = \frac{4\pi}{5} \frac{\sqrt{Q_{20}^2 + Q_{22}^2}}{A r_{\rm rms}^2} \ . \qquad (12)$$

The corresponding energies are found, respectively, at about $E = 3.0$, 6.5 and 15.3 MeV above the ground state. There is a clear correspondence with the shape of the potential energy surface of the LSD model where similar minima are found, respectively, at $\beta = 0.38$, 0.71 and 1.01 with energies $E = 2.3$, 6.6 and 8.9 MeV above the ground-state. Despite some quantitative differences, one can notice an equivalence in the structure of this nucleus in both descriptions.

IV. HIGHER DEFORMATIONS EFFECT

Since essentially no triaxial local minima have been found in the studied nuclei, apart from ^{184}Hg and ^{186}Hg, we only show the influence of the a_3 and a_4 deformations on the SPES in the axially symmetric case ($\gamma = 0$). Let us take the illustrative example of the SPES calculated for the nucleus ^{186}Hg (Fig. 7), where the non-axiality parameter γ has now been explicitly set to zero. In the upper part of Fig. 7, the SPES is plotted as a function of (β, a_3) assuming $a_4 = \beta^2/5$ which corresponds approximately to the bottom of the valley in the (β, a_4) plane. It is seen in Fig. 7 that the minimal-energy deformation is obtained for left-right symmetric shapes. Considering

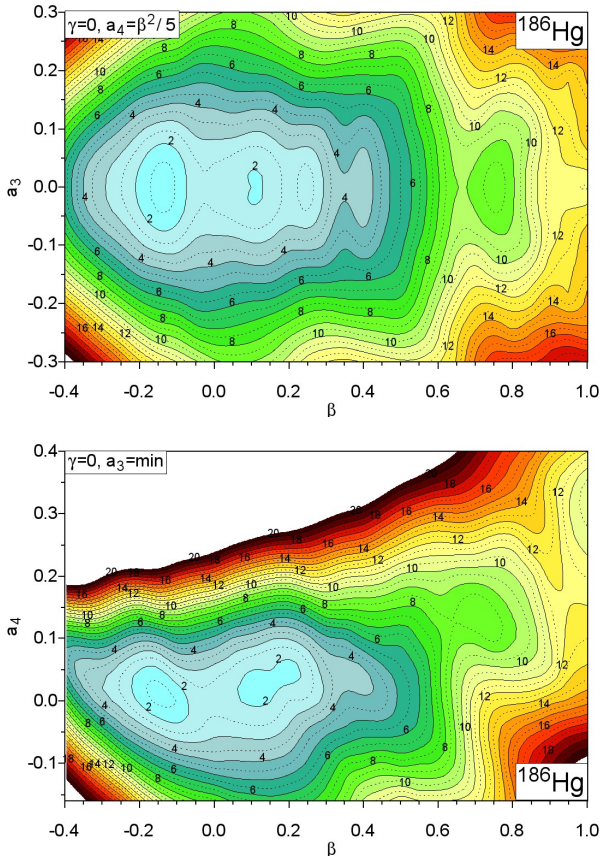

FIG. 7: Potential energy surface of ^{186}Hg for the axially symmetric case ($\gamma = 0$) as function of β and a_3 (upper map) and of β and a_4 (lower map).

only this figure, one would be tempted to conclude the possible presence of two minimal-energy configurations, corresponding one to a prolate ($\beta \approx 0.20$) and the other to an oblate shape ($\beta \approx 0.15$ separated by a barrier of about 0.5 MeV. However, a minimization with respect to the parameters a_3 and a_4, as shown in Fig. 4, does not support the existence of a prolate minimum. The tendency to form a rather elongated prolate shape around ($\beta \approx 0.725$), clearly visible in Fig. 7, seems, on the contrary, to be confirmed by a minimization calculation with respect to a_3 and a_4, as shown in Fig. 4 and described above. Another minimum similar to the one visible in Fig. 6 at Q_{20}=70 b is formed at $\beta > 1.0$ in Fig. 7.

V. SUMMARY AND CONCLUSION

In our study of shape isomers in even-even nuclei of the isotopic chains of Pt, Hg, and Pb around ^{186}Hg, a certain number of general remarks should be made. First of all, we have found that the left-right asymmetry degree of freedom does not play any important role in any of the here-considered nuclei, and this not only around the ground state but throughout the whole range of deformations, as long as the elongation does not become too large ($\beta < 0.6$). Let us mention at this point, however, that this conclusion does not necessarily hold when going to very large elongations, as it is well known that the left-right asymmetry becomes important for elongations encountered in the fission process. On the contrary, the minimization of the SPESs with respect to the neck deformation parameter a_4 makes the ground state minima in Pt and Hg isotopes deeper. It is, therefore, important for the study of shape isomers.

A prolate-oblate shape coexistence has been shown to be possible in the considered Pt and Hg isotopes, where the ground-state deformation is found on the prolate side in the platinium isotopes with a tendency, with increasing mass number, towards triaxial shapes (increasing γ value). In all three platinium isotopes, a clearly identified oblate shape isomer is found around $\beta \approx 0.18$.

In the neighboring mercury isotopes, the ground-state deformation is found on the oblate side, with a prolate shape isomer. With increasing mass numbers, the ground state becomes successively deeper while the prolate shape isomer gets shallower. In all three mercury isotopes, triaxial shape isomeric states are found around $\gamma \approx 20^\circ$ at an elongation of $\beta \approx 0.5$.

In the lead isotopes, the ground-state deformation has clearly shifted towards a spherical shape with an oblate shape-isomeric state around $\beta \approx 0.2$ and a prolate shape isomer that develops with increasing mass number at an elongation of $\beta \approx 0.45$. A triaxial shape isomer is found in all three lead isotopes at $\{\beta \approx 0.2, \gamma \approx 30^\circ\}$

Future investigations of other nuclear isotopic chains in the $Z \approx 82$ and other very different mass regions should be considered to probe, from a comparison with the experimental data, the predictive power of our theoretical approach.

Acknowledgements

Our research was supported by the Polish-French agreement COPIN-IN2P3: project No. 08-131 and 15-149 and also funded in part by the National Science Centre, Poland under research project No. 2023/49/B/ST2/01294.

[1] C. M. Polikanov et al., Zh. Eksp. Teor. Fiz. **42**, 1464 (1962) [Sov. Phys.- JETP **15**, 1016 (1962)].
[2] J. L. Wood, and K. Heyde, J. Phys. **G43**, 020402 (2016).
[3] P. E. Garrett, M. Zielinska, E. Clément, Prog. Part. Nucl. Phys. **124**, 103931 (2022).
[4] Y. L. Yang, P. W. Zhao, Z. P. Li , Phys. Rev. **C107**, 024308 (2023).
[5] D. Bonatsos, A. Martinou, S. K. Peroulis, T. J. Mertzimekis, N. Minkov, J. Phys. **G50**, 075105 (2023).
[6] D. Bonatsos, A. Martinou, S. K. Peroulis, T. J. Mertzimekis, N. Minkov, Atoms **11**, 117 (2023).
[7] P. M. Walker, A. K. Jain, B. Maheshwari, Eur. Phys. J. Spec. Top. **233**, 889 (2024).
[8] S. Leoni, B. Fornal, N. Marginean, M. Sferrazza, et al., Phys. Rev. Lett. **118**, 162502 (2017).
[9] S. Leoni, B. Fornal, N. Marginean, J. N. Wilson, Eur. Phys. J. Spec. Top. **233**, 1061 (2024).
[10] P. Bonche, S. J. Krieger, P. Quentin, M. S. Weiss, J. Meyer, M. Meyer, N. Redon, H. Flocard, P.-H. Heenen, et al., Nucl. Phys. **A500**, 308 (1989).
[11] M. Girod, J. P. Delaroche, D. Gogny, J. F. Berger, Phys. Rev. Lett. **62**, 2452 (1989).
[12] P. Möller, A. J. Sierk, R. Bengtsson, H. Sagawa, T. Ichikawa, Phys. Rev. Lett. **103**, 212501 (2009).
[13] P. Möller, A. J. Sierk, R. Bengtsson, H. Sagawa, T. Ichikawa, **98**, 149 (2012).
[14] J.A. Lay, A. Vitturi, L. Fortunato, Y. Tsunoda, T. Togashi, T. Otsuka, Phys. Lett. **B 838**, 137719 (2023).
[15] B. Olaizola, L.M. Fraile, H. Mach, A. Poves, F. Nowacki, A. Aprahamian, et al., Phys. Rev. **C 95**, (2017) 061303(R).
[16] B. Cederwall, R. Wyss, A. Johnson, J. Nyberg, B. Fant, R. Chapman, D. Clarke, F. Khazaie, et al., Z. Phys. **337**, 292 (1990).
[17] A. N. Andreyev, M. Huyse, P. Van Duppen, L. Weissman, D. Ackermann, F. P. Hessberger, S. Hofmann, A. Kleinböhl, G. M. Münzenberg et al., Nature **405**, 430 (2000).
[18] K. Heyde and J.L. Wood, Rev. Mod. Phys. **83**, 1467 (2011).
[19] J.M. Yao, M. Bender, and P.-H. Heenen, Phys. Rev. C **87** 034322 (2013).
[20] A. Poves, J. Phys. **G43**, 020401 (2016).
[21] B. Nerlo-Pomorska, K. Pomorski, J. Bartel, and C. Schmitt, Eur. Phys. J. **A53**, 67 (2017).
[22] Zs. Podolyák, Journ. Phys. Conf. Ser. **381**, 012052 (2012).
[23] R. Julin, T. Grahn, J. Pakarinen, P. Rahkila, Journ. Phys. G **43**, 024004, (2016).
[24] K. Wrzosek-Lipska, L. P. Gaffney, Journ. Phys. G **43**, 024012 (2016).
[25] M. Bender, P.-H. Heenen, P.-G. Reinhard, Rev. Mod. Phys. **75**, 121 (2003).
[26] K. Nomura, R. Rodriguez-Guzman, L. M. Robledo, Phys. Rev. C **87**, 064313 (2013).
[27] T. Niksić, D. Vretenar, P. Ring, G. A. Lalazissis, Phys. Rev. C **65**, 054320 (2002).
[28] K. Pomorski, B. Nerlo-Pomorska, A. Dobrowolski, J. Bartel, C. M. Petrache, Eur. Phys. Journ. **A56**, 107 (2020).
[29] K. Pomorski, B. Nerlo-Pomorska, Acta Phys. Pol. **B Suppl. 4-A21 16**, (2023).

[30] K. Pomorski, B. Nerlo-Pomorska, J. Bartel, C. Schmitt, Z. G. Xiao, Y. J. Chen, L. L. Liu, Phys. Rev. C **110**, 034607 (2024).
[31] K. Pomorski, J. Dudek, Phys. Rev. C **67**, 044316 (2003).
[32] K. T. R. Davies and J. R. Nix, Phys. Rev. C **14**, 1977 (1976).
[33] A. Dobrowolski, K. Pomorski, J. Bartel, Comp. Phys. Comm. **199**, 118 (2016).
[34] C. Schmitt, K. Pomorski, B. Nerlo-Pomorska, J. Bartel, Phys. Rev. **C95**, 034612 (2017).
[35] Å. Bohr, Mat. Fys. Medd. Dan. Vid. Selsk. **26**, no. 14 (1952).
[36] S.G. Rohoziński, A. Sobiczewski, Acta. Phys. Polon. B **12**, 1001 (1981).
[37] W. D. Myers, W. J. Świątecki, Nucl. Phys. **81**, 1 (1966).
[38] V. M. Strutinsky, Sov. J. Nucl. Phys. **3**, 449 (1966); Nucl. Phys. A **95**, 420 (1967); Nucl. Phys. A **122**, 1 (1968).
[39] S. G. Nilsson, C. F. Tsang, A. Sobiczewski, Z. Szymański, S. Wycech, S. Gustafson, I. L. Lamm, P. Möller, B. Nilsson, Nucl. Phys. A **131**, 1 (1969).
[40] J. Bardeen, L. N. Cooper, J. R. Schrieffer, Phys. Rev. **108**, 1175 (1957).
[41] A. Góźdź, K. Pomorski, Nucl. Phys. A **451**, 1 (1986).
[42] S. Piłat, K. Pomorski, A. Staszczak, Zeit. Phys. A **332**, 259 (1989).
[43] P. Möller, J. R. Nix, Data Nucl. Data Tables **59**, 185 (1995).
[44] J.F. Berger, J. Girod, and D. Gogny, Nucl. Phys. A **428**, 23c (1984).
[45] K. Heyde, P. V. Isacker, M. Waroquier, J. L. Wood, R. A. Meyer, Phys. Rep. **102**, 291 (1983).
[46] L. M. Robledo, R. Rodríguez-Guzmán and P. Sarriguren, J. Phys. G: Nucl. Part. Phys. **36** 115104 (2009)
[47] R. Rodríguez-Guzmán, P. Sarriguren, L. M. Robledo, and J. E. García-Ramos Phys. Rev. C **81**, 024310 (2010)